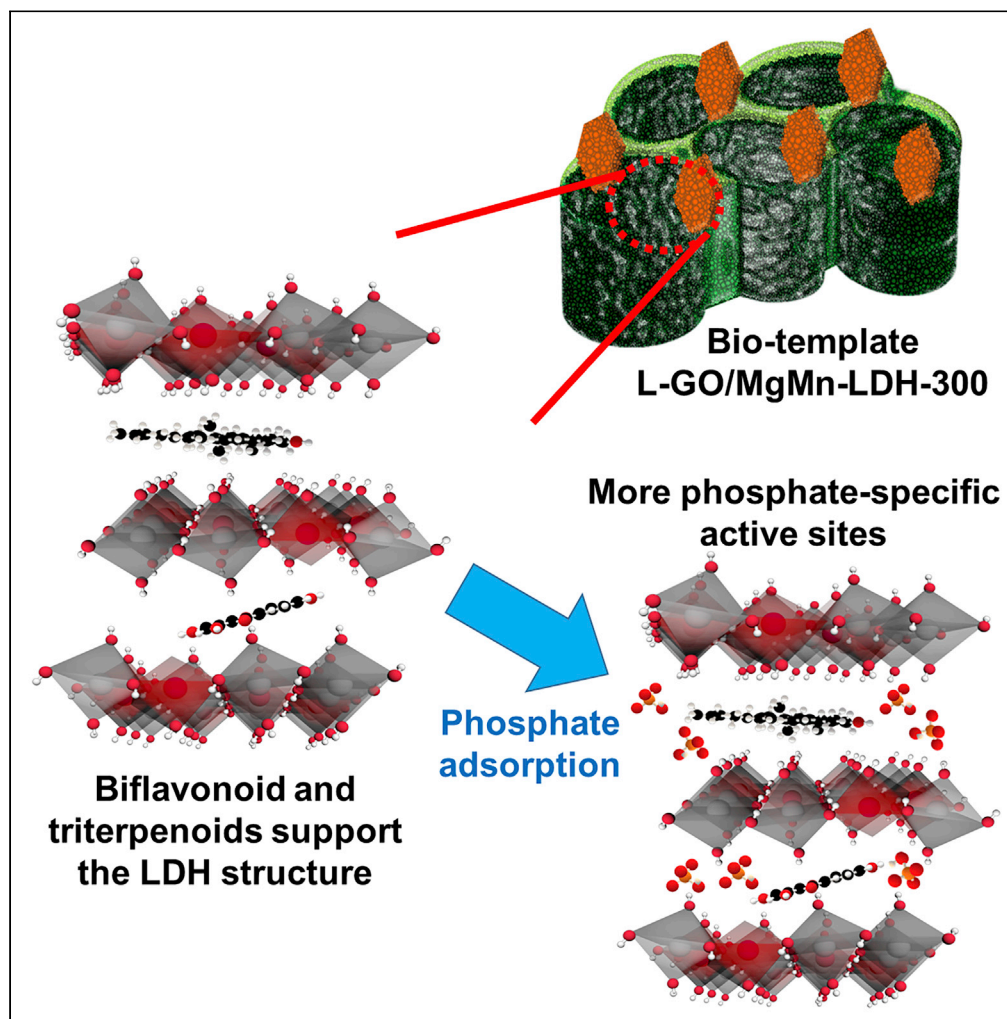


## Article

## Green Treatment of Phosphate from Wastewater Using a Porous Bio-Templated Graphene Oxide/MgMn-Layered Double Hydroxide Composite



Yi-Ting Lai, Yu-Sheng Huang, Chin-Hsuan Chen, ..., Chi-Young Lee, Po-Chun Hsu, Nyan-Hwa Tai

pochun.hsu@duke.edu (P.-C.H.)  
nhtai@mx.nthu.edu.tw (N.-H.T.)

**HIGHLIGHTS**  
A natural bio-template provides hierarchical porous structure

The variation of nanostructure during thermal process is discussed in detail

The composite shows high sorption, selectivity, stability, and sustainability

Lai et al., iScience 23, 101065  
May 22, 2020 © 2020 The Authors.  
<https://doi.org/10.1016/j.isci.2020.101065>



## Article

# Green Treatment of Phosphate from Wastewater Using a Porous Bio-Templated Graphene Oxide/MgMn-Layered Double Hydroxide Composite

Yi-Ting Lai,<sup>1,2</sup> Yu-Sheng Huang,<sup>1</sup> Chin-Hsuan Chen,<sup>3</sup> Yan-Cheng Lin,<sup>1</sup> Horng-Tay Jeng,<sup>3,4,5</sup> Min-Chao Chang,<sup>6</sup> Lih-Juann Chen,<sup>1</sup> Chi-Young Lee,<sup>1</sup> Po-Chun Hsu,<sup>2,\*</sup> and Nyan-Hwa Tai<sup>1,7,\*</sup>

## SUMMARY

**Excessive phosphorus in water is the primary culprit for eutrophication, which causes approximately \$2.2 billion annual economic loss in the United States. This study demonstrates a phosphate-selective sustainable method by adopting *Garcinia subelliptica* leaves as a natural bio-template, where MgMn-layered double hydroxide (MgMn-LDH) and graphene oxide (GO) can be grown *in situ* to obtain L-GO/MgMn-LDH. After calcination, the composite shows a hierarchical porous structure and selective recognition of phosphate, which achieves significantly high and recyclable selective phosphate adsorption capacity and desorption rate of 244.08 mg-P g<sup>-1</sup> and 85.8%, respectively. The detail variation of LDHs during calcination has been observed via *in situ* transmission electron microscope (TEM). Moreover, the roles in facilitating phosphate adsorption and antimicrobial ability of chemical constituents in *Garcinia subelliptica* leaves, biflavonoids, and triterpenoids have been investigated. These results indicate the proposed bio-templated adsorbent is practical and eco-friendly for phosphorus sustainability in commercial wastewater treatment.**

## INTRODUCTION

With the rapid population growth and exacerbating chemical pollution, clean water has become a critical demand all over the world. Thus, how to develop efficient and effective technology of wastewater treatment has become one of the major challenges for scientists from various fields (Zhang et al., 2018) (Lai et al., 2019b; Li et al., 2018b; Lin et al., 2019); Liu et al. (2017) (Liu et al., 2019; Wan and Chung, 2018); Phosphate is often present in wastewater due to the industrial, agricultural, and household activities and can lead to water eutrophication and endanger aquatic creatures (Ooi et al., 2017; Ren et al., 2012). There are over 90% of ecoregion rivers exceeding reference median values of total phosphorus concentration announced by the US Environmental Protection Agency and about \$2.2 billion annual economic loss due to eutrophication in the US freshwaters (Dodds et al., 2009). Considering that phosphate is an essential and limited element and is widely used in agriculture and various industries, it is imperative to develop technologies that can separate and recycle phosphate from wastewater to not only reduce the impact on the environment but also produce more resources of fresh water and phosphate. Recently, various researches such as crystallization (Peng et al., 2018), membrane process (Thong et al., 2016), electrodialysis (Zhang et al., 2013), and chemical and biological methods have been proposed for removal of phosphate from wastewater (Li et al., 2016a; Seviour et al., 2003). Adsorption method is considered as one of the most practical techniques because it possesses high efficiency, simplicity, and cost-effectiveness and does not produce other hazardous waste. In this regard, various kinds of materials have been applied as adsorbents, including layered double hydroxides (LDHs) (Mandel et al., 2013), carbon materials (Li et al., 2016c), polymers (Zhao et al., 2018), and metal-organic frameworks (Li et al., 2018a), to remove pollutants from wastewater.

LDHs, composed of lamellar hydroxides of divalent ( $M_{II}^{2+}$ ) and partially substituted trivalent ( $M_{III}^{3+}$ ) cations, have attracted great attention as green and sustainable materials for applications in removing environmental substances, organic molecule degradation, and energy production (Arrabito et al., 2019; Gu et al., 2018; Wang and O'Hare, 2012). Its general formula is  $[M_{I}^{2+}_{1-x}M_{II}^{3+}_x(OH)_2]^{x+}[A^{y-}]_{x/y}\cdot nH_2O$ , in which A represents internal exchangeable anions to balance the overall charge (Shao et al., 2015). Various

<sup>1</sup>Department of Materials Science and Engineering, National Tsing-Hua University, Hsinchu, Taiwan 30013, Republic of China

<sup>2</sup>Department of Mechanical Engineering and Materials Science, Duke University, Durham, NC 27708, USA

<sup>3</sup>Department of Physics, National Tsing-Hua University, Hsinchu, Taiwan 30013, Republic of China

<sup>4</sup>Physics Division, National Center for Theoretical Sciences, Hsinchu, Taiwan 30013, Republic of China

<sup>5</sup>Institute of Physics, Academia Sinica, Taipei, Taiwan 11529, Republic of China

<sup>6</sup>Material and Chemical Research Laboratories, Industrial Technology Research Institute, Hsinchu Taiwan 30011, Republic of China

<sup>7</sup>Lead Contact

\*Correspondence:  
[\(P.-C.H.\),](mailto:pochun.hsu@duke.edu)  
[\(N.-H.T.\)](mailto:nhtai@mx.nthu.edu.tw)

<https://doi.org/10.1016/j.isci.2020.101065>



compositions of LDHs have been reported as promising materials for phosphate removal owing to their chemical stability, structure memory effect, and high anion exchange capacity (Zhou et al., 2011). Yang et al. prepared Mg-Al and Zn-Al LDHs as adsorbents for phosphate removal, where the adsorption mechanism was thoroughly investigated (Yang et al., 2014). Shimamura et al. proposed a model to explain the thermal behavior of ion exchange using Mg/Al-LDH with interlayer phosphate (Shimamura et al., 2012). However, there is still an imperative demand to develop an economical synthesis method of LDHs for phosphate uptake with high surface area, selectivity, and adsorption capacity.

Carbon materials such as active carbon, carbon nanotubes, and graphene have been widely used as adsorbents for removal of various pollutants in wastewater treatment (Davood Abadi Farahani et al., 2018; Wu et al., 2019). Notably, the two-dimensional graphene oxide (GO) possesses high adsorptive capacity owing to its high specific surface area and a great number of binding sites (Mao et al., 2019; Li et al., 2019). In addition, solution-based GO fabrication methods are straightforward and economic, which makes them suitable for large-scale production. However, the low selectivity of GO for phosphate uptake limits the application for practical wastewater treatment. Previous research has reported that using GO combined with various materials for phosphate adsorption, such as titania (Sakulpaisan et al., 2016),  $\text{Fe}_2\text{O}_3$  (Bai et al., 2018), and  $\text{ZrO}_2$  (Luo et al., 2016).

In our previous work, a GO/MgMn-layered double hydroxide (MgMn-LDH) composite calcined at 300°C (GO/MgMn-LDH-300) was prepared for the uptake and release of phosphate in wastewater treatment (Lai et al., 2019a). The mechanism of phosphate removal in the presence of GO was investigated in detail. In this context, to further enhance the adsorption efficiency, it is crucial to provide a hierarchical porous structure. Herein we develop a novel adsorbent utilizing *Garcinia subelliptica* leaves as a bio-derived template. MgMn-LDH was *in situ* grown on the leaf-templated GO (L-GO) to obtain L-GO/MgMn-LDH and its calcined sample (L-GO/MgMn-LDH-300), as shown in Figure 1A. Leaves possess a natural hierarchical porous structure, which is composed of many fibers and vessels and can serve as a potential bio-template (Yang et al., 2013). To the best of our knowledge, most of the previous studies indicate that calcination of LDHs results in the collapse of the layered structure and formation of amorphous structures, which is corroborated by X-ray diffraction (XRD) results (Goh et al., 2008; Yan et al., 2016). Here, in this study, we proposed a new finding that recrystallization of MgMn-LDH occurred and led to a more hierarchical porous structure in the presence of *Garcinia subelliptica* leaves after calcination at 300°C. *In situ* transmission electron microscopy (TEM) and high-resolution (HR) TEM have been conducted to directly observe and characterize the variations of nanostructures. In addition, the intercalated biflavonoids and triterpenoids can enlarge the LDH layer distance and produce phosphate-specific active sites for phosphate adsorption as illustrated in Figure 1B. The fabricated L-GO/MgMn-LDH-300 not only shows high adsorption capacity of phosphate but also possesses the antimicrobial property. This work demonstrates a novel adsorbent for the effective recycling phosphate from aqueous solutions, adopting *Garcinia subelliptica* leaves as an inexpensive and natural template, which is scalable, sustainable, and suitable in commercial wastewater treatment.

## RESULTS

### Characterizations of the Hierarchical Porous Structure of LDH Composites

Field emission scanning electron microscope (FESEM) images were used to observe the morphological evolution of the procedure for the preparation of L-GO/MgMn-LDH-300. Figure 2A shows that *Garcinia subelliptica* leaves possess a natural three-dimensional (3D) hierarchical porous structure (the inset is a higher-magnification FESEM image). As shown in Figure 2B, L-GO successfully exhibited the natural leaf's 3D porous structure after GO coating. The leaf skeleton was covered by GO layers with folding edges and wrinkles, as shown in the inset of Figure 2B. Figure 2C and its inset show that the plate-like MgMn-LDHs were *in situ* coated on L-GO/MgMn-LDH composite's surface. Figure 2D indicates that L-GO/MgMn-LDH-300 composite remained the 3D porous structure of the leaf template. The inset of Figure 2D shows that numerous mesopores formed after calcination at 300°C. The hierarchical porous structure can provide more active sites and result in more efficient ion transport for phosphate adsorption. The morphology and element distributions of L-GO/MgMn-LDH-300 were further analyzed by TEM images, as shown in Figure S1.

The typical  $\text{N}_2$  adsorption-desorption isotherms of the LDH composites for the characterization of specific surface area were illustrated in Figure 2E. The isotherms of L-GO/MgMn-LDH-300 show a combination of type II and type IV curves, indicating the presence of meso/macropores among this porous structure (Cheng et al., 2018). In particular, the leaf-templated LDH composite shows a H4 hysteresis loop at medium

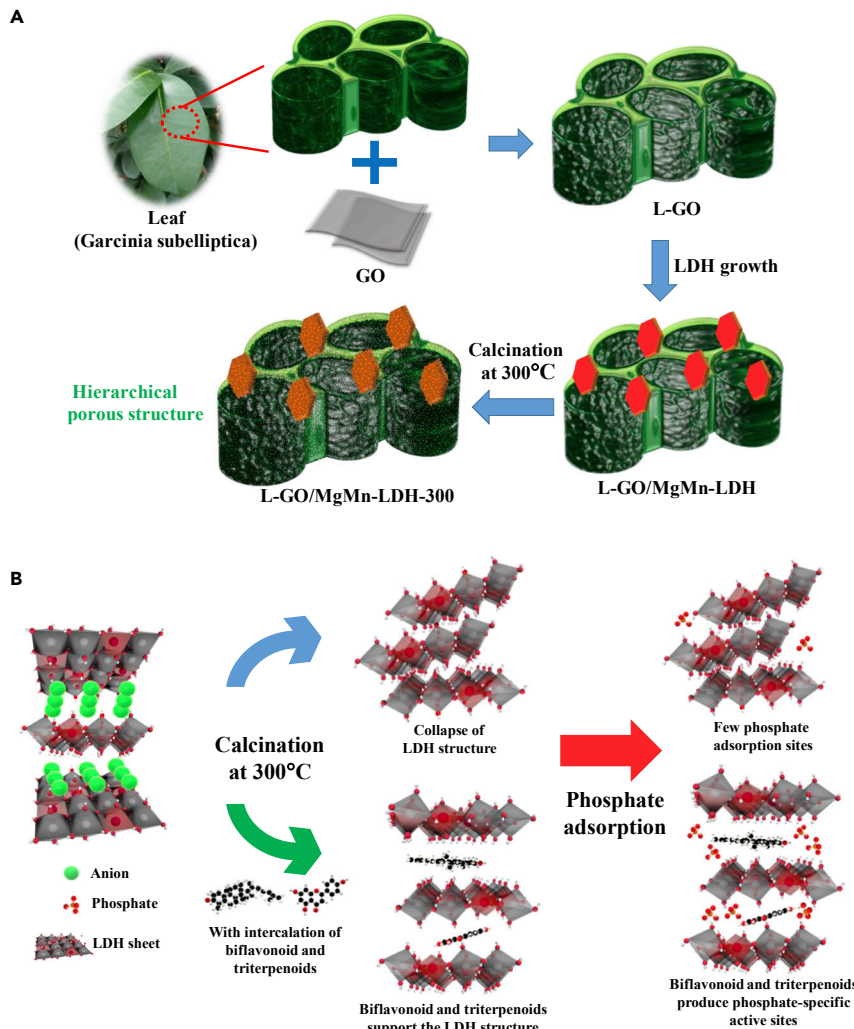


**Figure 1. Schematic Diagram of the Procedure for Preparation of L-GO/MgMn-LDH-300 and Mechanisms of Selective Phosphate Adsorption**

(A) The bio-templated LDH composites can produce a more hierarchical porous structure after calcination.

(B) The mechanisms for the enhancement of selective-phosphate adsorption capacity of L-GO/MgMn-LDH-300. The presence of intercalated biflavonoids and triterpenoids can not only increase and support the LDH layer distance during calcination but also form bonding with phosphate to facilitate the selective phosphate adsorption.

$P/P_0$ , which demonstrates the presence of microporous structure. The pore size distributions of the LDH composites are displayed in Figure 2F. The L-GO/MgMn-LDH-300 exhibits a hierarchical porous structure ranging from about 1.5 nm to more than 400 nm. Notably, the L-GO/MgMn-LDH-300 possesses a high volume of mesopores and specific surface area of  $91.39 \text{ m}^2 \text{ g}^{-1}$ , as shown in Figure S2 and Table S1, respectively. The higher surface area and mesopore ratio of an adsorbent provide more adsorption sites and rapid ion transfer, which facilitates phosphate adsorption process.

### Characterizations of the Compositions of LDH Composites

Fourier transform infrared (FTIR) analysis was conducted to characterize the compositions of the LDH composites. As shown in Figure 3A, the adsorption bands of stretching and bending vibration of the interlayer water molecules are located at  $3,350$  and  $1,630 \text{ cm}^{-1}$ , respectively. The band at approximately  $1,380 \text{ cm}^{-1}$  is assigned to functional groups on GO (C-H and C=O stretching vibrations) and carbonate anions in the interlayer space (Yang et al., 2014). The band at  $850 \text{ cm}^{-1}$  results from the M-O bending (M = metal) (Xu et al., 2014). In addition, the main bands at the same positions are observed in the FTIR spectra of *Garcinia*

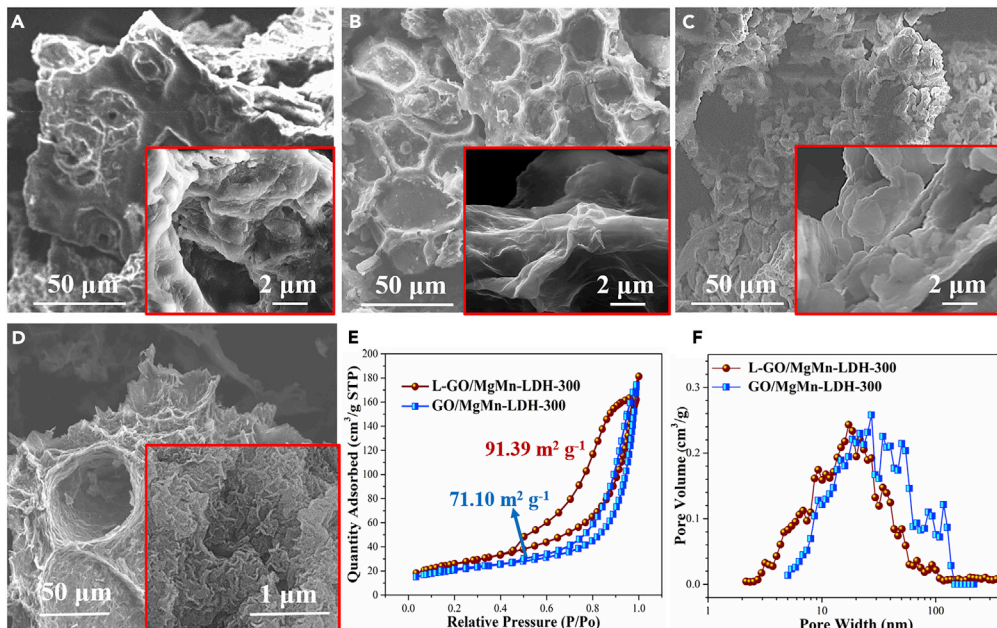


**Figure 2. Characterizations of the Hierarchical Porous Structure of LDH Composites**

(A–D) FESEM images of the LDH composites: (A) *Garcinia subelliptica* leaves, (B) L-GO, (C) L-GO/MgMn-LDH, and (D) L-GO/MgMn-LDH-300 composites. Insets are the higher-magnification FESEM images, which show that numerous mesopores formed after calcination.

(E) The typical  $N_2$  adsorption-desorption isotherms of LDH composites.

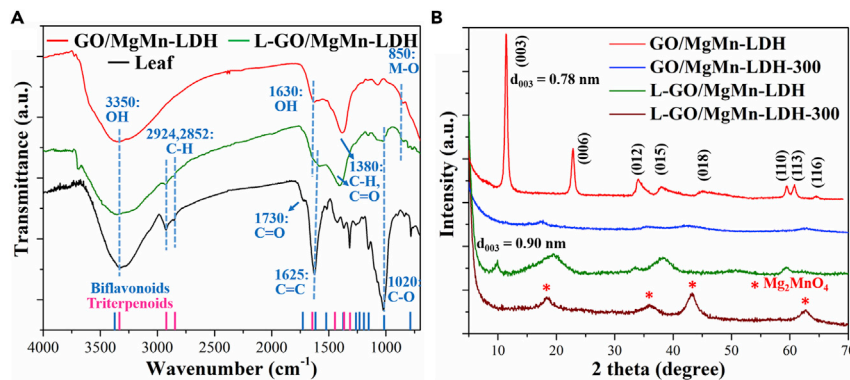
(F) Pore size distributions of L-GO/MgMn-LDH-300 and GO/MgMn-LDH-300 composites. The L-GO/MgMn-LDH-300 possesses high mesopores ratio and specific surface area of  $91.39\text{ m}^2\text{ g}^{-1}$ .

*subelliptica* leaves and L-GO/MgMn-LDH. The bands at  $2,924$  and  $2,852\text{ cm}^{-1}$  are attributed to the C-H stretching of alkane. The band at  $1,625\text{ cm}^{-1}$  is due to the presence of  $\alpha$ ,  $\beta$ -unsaturated ketone and aromatic bonding. The strong band at  $1,020\text{ cm}^{-1}$  is ascribed to the C-O stretching of alkyl aryl ether. These results correspond to the FTIR spectra of biflavonoids and triterpenoids, which are the major compounds of *Garcinia subelliptica* leaves (Inoue et al., 2017; Ito et al., 2013; Kedar Kalyani Abhimanyu, 2012). It is suggested that biflavonoids and triterpenoids are present in L-GO/MgMn-LDH.

As shown in Figure 3B, XRD pattern of GO/MgMn-LDH reveals dominant and symmetric peaks of (003) and (006), which are regarded as the basal planes, and the asymmetric peaks of (012), (015), and (018) indicate the reflections of non-basal planes. The peaks of (110) and (113) are referred to as the distance of metal hydroxide layers. These reflections indicate the hexagonal lattice with rhombohedral  $R\bar{3}m$  symmetry of typical LDHs (Li et al., 2017; Yang et al., 2014). Comparing with GO/MgMn-LDH, the broad XRD peaks of L-GO/MgMn-LDH indicate the loose crystal structure. The basal spacing  $d_{003}$  of  $0.78\text{ nm}$  at  $2\theta = 11.41^\circ$  increases to  $0.90\text{ nm}$  at a lower angle of  $9.93^\circ$  for L-GO/MgMn-LDH. The same value of  $d_{110}$ , related to the distances and ordering of the metal hydroxide layers, shows the same chemical formula for the GO/MgMn-LDH and L-GO/MgMn-LDH (Mandel et al., 2013). It indicates that the increase of interlayer spacing and the weakening of the crystallinity for L-GO/MgMn-LDH result from the intercalation of biflavonoids and triterpenoids, which agree with the results of FTIR spectra. The increase in the interlayer spacing can facilitate ion access to the LDH composite, contributing to a higher phosphate adsorption capacity. After calcination at  $300^\circ\text{C}$  for 4 h, interlayer molecules were removed, resulting in collapsing of the layered structure and leading to the amorphous structure of the GO/MgMn-LDH-300, as illustrated in Figure 1B. In contrast, new peaks corresponding to  $\text{Mg}_2\text{MnO}_4$  appeared for the L-GO/MgMn-LDH-300 (JCPDS No. 19–0773), suggesting the formation of new oxide phases.

### Characterizations of the Variations of Nanostructures by *In Situ* TEM

Calcination is reported to be an essential factor to affect the anion adsorption by LDHs (Goh et al., 2008). Medaglia et al. proposed an emerging intense UV photoluminescence in Zn/Al LDH, which was activated by thermal

**Figure 3. FTIR and XRD Analyses of Materials**

(A) FTIR spectra of *Garcinia subelliptica* leaves, GO/MgMn-LDH, and L-GO/MgMn-LDH. The peaks in L-GO/MgMn-LDH agree with those of *Garcinia subelliptica* leaves, indicating the presence of biflavonoids and triterpenoids.

(B) XRD patterns of GO/MgMn-LDH, L-GO/MgMn-LDH, and their calcined samples. The increase of  $d_{003}$  layer space of L-GO/MgMn-LDH (from 0.78 to 0.90 nm) suggests the intercalation of biflavonoids and triterpenoids. After calcination, L-GO/MgMn-LDH-300 formed new oxide phase of  $\text{Mg}_2\text{MnO}_4$ , whereas GO/MgMn-LDH-300 showed amorphous phase owing to collapse of the layer structure.

dehydration (Prestopino et al., 2019). It clearly shows that thermal desorption of interlayer water results in the progressive collapse of LDHs. While the calcination temperature is over 300°C, undesired oxide phases form and decrease the phosphate adsorption capacity. The effects of calcination temperature on the phosphate absorption had been discussed in Tezuka's work (Satoko et al., 2004). Therefore, the calcination temperature of 300°C was chosen in this study, which resulted in the collapse of the layered structure of L-GO/MgMn-LDH-300. The *in situ* TEM provides important information to observe and characterize the variations of nanostructures of L-GO/MgMn-LDH composite during calcination (see Video S1). Figures 4A and 4B show the TEM and the selected area electron diffraction pattern (SAED) images of L-GO/MgMn-LDH composite before and after thermal process by *in situ* TEM. In Figure 4A, the inset of SAED pattern shows broad concentric rings with diffused halos, which could be attributed to MnO in loose MgMn-LDH structure. After thermal treatment at 300°C, mesopores appear in Figure 4B, suggesting the formation of hierarchical porous structure of L-GO/MgMn-LDH-300 during thermal treatment. In addition, new diffraction rings emerge in the SAED pattern, which can be ascribed to (311), (220), and (111) planes of  $\text{Mg}_2\text{MnO}_4$ , which confirms the results of XRD. Figure 4C presents the annular bright-field (ABF) scanning transmission electron microscope (STEM) image of L-GO/MgMn-LDH-300 to further characterize the mechanism of forming a hierarchical porous structure. It shows that the mesopores with the diameter of 3–20 nm (pointed out by orange arrows) are surrounded by  $\text{Mg}_2\text{MnO}_4$  nanoparticles. Figure S3 shows the energy dispersive X-ray spectra for elemental analysis of the large area and the crystallization part of L-GO/MgMn-LDH-300 composite. It indicates that the Mg:Mn ratio of 3:1 for overall large area decreases to near 2:1 in the crystallization part, which can be attributed to the formation of  $\text{Mg}_2\text{MnO}_4$ . High-angle annular dark-field (HAADF) STEM atomic image shown in Figure 4D reveals a lattice spacing of 4.76 Å of the nanocrystal, which shall correspond to the (1 1 -1) plane of  $\text{Mg}_2\text{MnO}_4$  phase. The diffraction pattern (inset) also proves the formation of  $\text{Mg}_2\text{MnO}_4$ . It is suggested that Mn elements tended to migrate and interact with oxygen-containing functional groups in GO and *Garcinia subelliptica* leaves during the calcination process and therefore were oxidized and formed the  $\text{Mg}_2\text{MnO}_4$  phase. Besides, numerous vacancies were generated as the by-product of oxidation in the *in situ* locations, which resulted in the formation of mesopores. These mesopores can not only contribute to the hierarchical porous structure but also facilitate the fast ion transfer of solution into the adsorbents for efficient phosphate adsorption process.

### Characterizations of the Elements and Bondings of the LDH Composites

X-ray photoelectron spectroscope (XPS) was used to characterize the elements and oxidation states of the LDH composites and bonding with the phosphate group. The high-resolution C 1s of *Garcinia subelliptica* leaves is present in Figure 5A. The strong peaks for C-O and C=O are attributed to the presence of biflavonoids and triterpenoids. After *in situ* coating of GO and growing LDH onto the leaves surface, the peak at approximately 289–290 eV representing for metal carbonate appeared (shown in Figure 5B), indicating the interaction with hydrocarbonate group and metal ions (Shchukarev and Korolkov, 2004). Figure 5C shows that L-GO/MgMn-LDH-300 possesses a more intensive peak of metal carbonate, implying that GO and

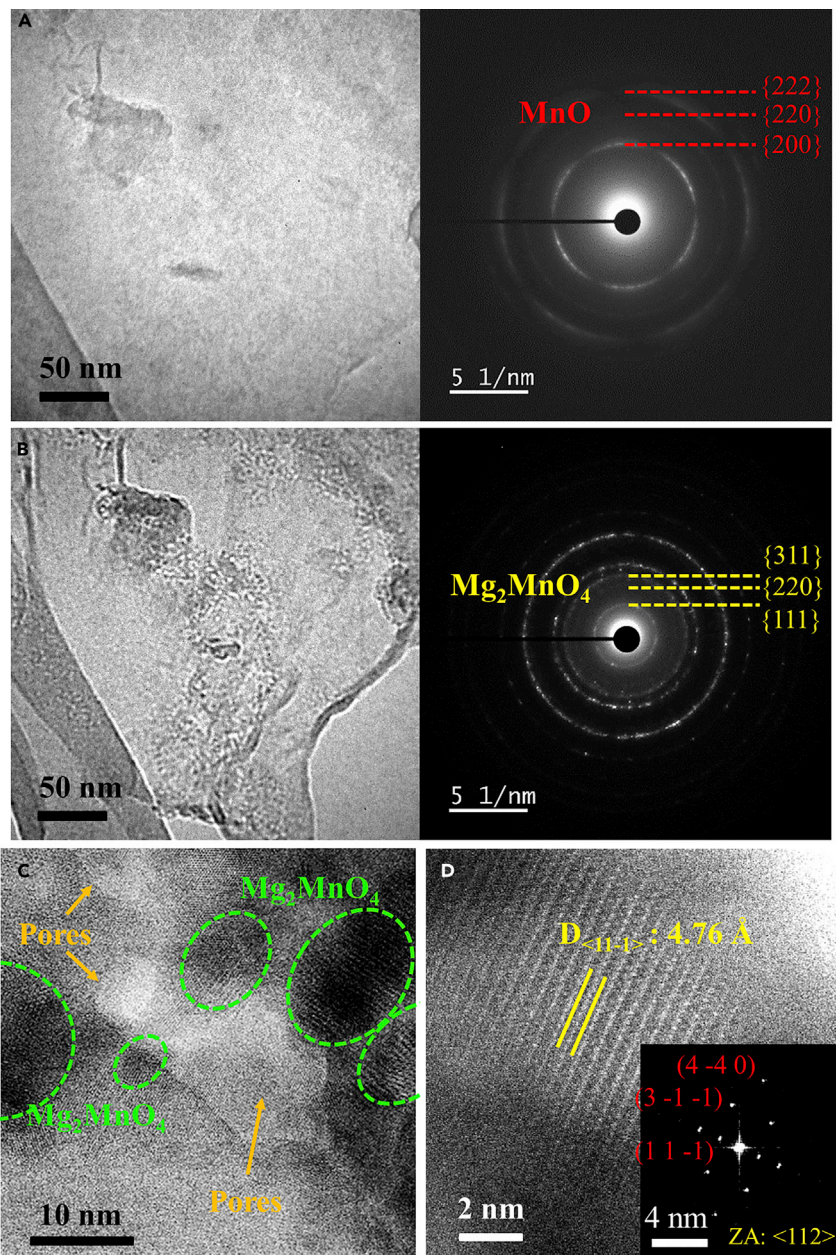


**Figure 4. Characterization of the Variations of Nanostructures by *In Situ* TEM**

(A and B) TEM images and SAED images (in the insets) of L-GO/MgMn-LDH composite (A) before thermal treatment and (B) after *in situ* thermal treatment at 300°C for 100 min.

(C) ABF STEM image of L-GO/MgMn-LDH-300, which presents mesopores (marked by orange arrows) and surrounding Mg<sub>2</sub>MnO<sub>4</sub> nanocrystals.

(D) HAADF STEM atomic images reveal the presence of Mg<sub>2</sub>MnO<sub>4</sub> phases with lattice spacing of 4.76 Å. Inset shows the diffraction pattern of the Mg<sub>2</sub>MnO<sub>4</sub>.

*Garcinia subelliptica* leaves with the associated abundant oxygen-containing functional groups facilitated the interaction with metal ions in the LDHs during calcination (Lai et al., 2019a). After adsorption of phosphate, the ratio of metal carbonate decreased from 16.4% to 7.1% of phosphate-loaded L-GO/MgMn-LDH-300 (P-L-GO/MgMn-LDH-300) as shown in Figure 5D. It indicates that the carbonate binding to LDH was replaced by phosphate through ion and ligand exchange (Luo et al., 2016). The peaks shown in Figures 5E and 5F correspond to the Mn 2p<sub>3/2</sub> state, which are used to determine the multivalent state of Mn in

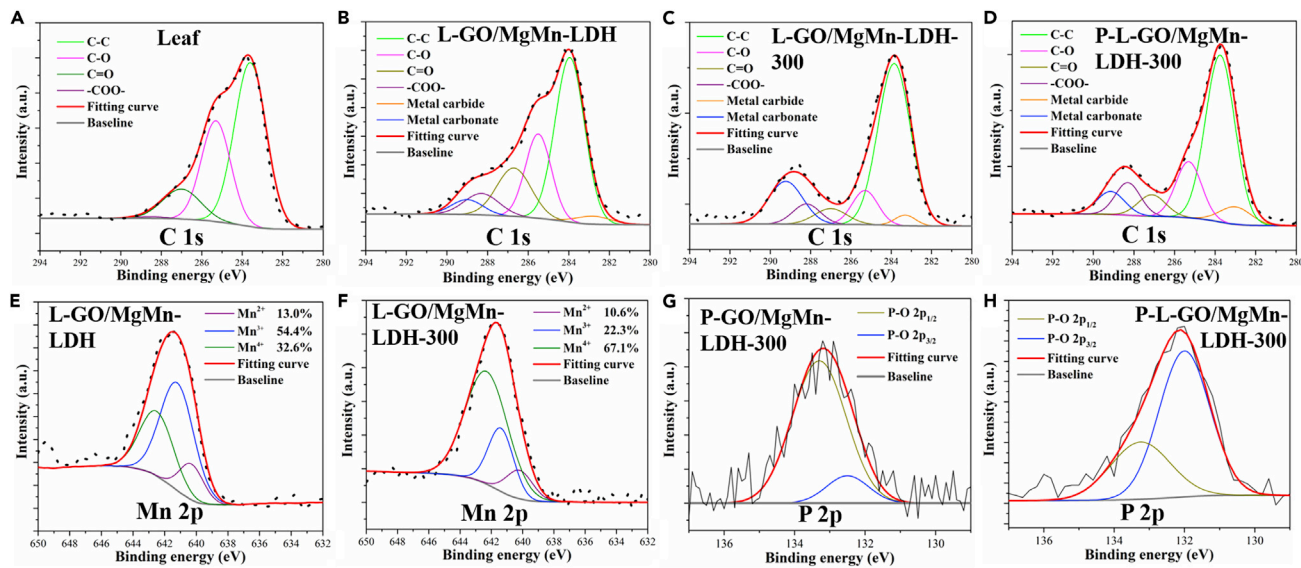


**Figure 5. Characterizations of the Elements and Bondings of the LDH Composites**

(A–D) XPS spectra of high resolution for C 1s. (A) *Garcinia subelliptica* leaves, (B) L-GO/MgMn-LDH, (C) L-GO/MgMn-LDH-300, and (D) phosphate-adsorbed L-GO/MgMn-LDH-300. The higher intensive peak of metal carbonate on L-GO/MgMn-LDH-300 reveals that the functional groups on GO and *Garcinia subelliptica* leaves facilitated the interaction with metal ions in the LDHs during calcination. The decrease of metal carbonate ratio on P-GO/MgMn-LDH-300 after phosphate adsorption indicates that the carbonate binding to LDH was replaced by phosphate through ion and ligand exchange. (E and F) The high-resolution Mn 2p peak of composites. (E) L-GO/MgMn-LDH and (F) L-GO/MgMn-LDH-300. The high oxidation state of Mn in the L-GO/MgMn-LDH-300 composite can produce more phosphate-specific adsorption sites. (G and H) The high resolution of P 2p of the (G) P-GO/MgMn-LDH-300 and (H) P-L-GO/MgMn-LDH-300. The downshift of P–O bonds indicates the higher electronic density of P 2p binding on P-L-GO/MgMn-LDH-300. It is suggested that P–O groups on phosphate can form bonding with aromatic hydrocarbons and the long pairs on biflavonoids and triterpenoids, which can facilitate the selective recognition of phosphate.

the LDH composites. The oxidation progress of Mn<sup>2+</sup> to Mn<sup>4+</sup> can be facilitated through calcination, which produced more phosphate-specific adsorption sites in the L-GO/MgMn-LDH-300 composite (Satoko et al., 2004). Figures 5G and 5H are the phosphate-loaded GO/MgMn-LDH-300 (P-GO/MgMn-LDH-300) and P-L-GO/MgMn-LDH-300, respectively. The peak at 133.3 eV was attributed to P–O bonds, which has a splitting value of ~0.84 eV for P 2p<sub>3/2</sub>–P 2p<sub>1/2</sub> (Susi et al., 2015). It is noted that the downshift of P–O bonds of P-L-GO/MgMn-LDH-300 is observed, indicating the higher electronic density of P 2p binding on P-L-GO/MgMn-LDH-300 than that on P-GO/MgMn-LDH-300. It is assumed that the P–O groups on phosphate can form bonding with aromatic hydrocarbons and the long pairs on biflavonoids and triterpenoids. The formation of the above bondings can facilitate the selective recognition of phosphate, which contributes to high selective phosphate adsorption capacity for L-GO/MgMn-LDH-300.

### Analyses of Practical Phosphate Sustainability in Wastewater

The time-dependence phosphate adsorption capacities of the GO/MgMn-LDH-300 and L-GO/MgMn-LDH-300 composites are presented in Figure 6A. The GO/MgMn-LDH-300 demonstrated rapid phosphate adsorption in the first 1.5 h and subsequently reached equilibrium after 3 h. Its adsorption capacity reaches 44.50 mg-P g<sup>-1</sup> after 24 h. In sharp contrast, the L-GO/MgMn-LDH-300 not only showed even faster adsorption in the first 1.5 h, but also reached high phosphate adsorption capacity of 244.08 mg-P g<sup>-1</sup> after 24 h, which is 5.5 times that of the GO/MgMn-LDH-300 composite. The adsorption kinetics of LDH composites were investigated using the pseudo-first-order and pseudo-second-order models, which are shown in Figure S4 and summarized in Table 1. Both LDH composites exhibited higher correlation coefficients ( $R^2$ ) of the pseudo-second-order model, indicating that the phosphate adsorption processes of both adsorbents were dominated by chemisorption. It is noted that the proposed bio-templated L-GO/MgMn-LDH-300 exhibited an extremely high phosphate adsorption capacity as compared with the published research results, which were summarized in Table 2.

The selectivity of phosphate adsorption by L-GO/MgMn-LDH-300 was investigated in the presence of competing ions. A 200 mL solution containing HPO<sub>4</sub><sup>2-</sup>, Cl<sup>-</sup>, SO<sub>4</sub><sup>2-</sup>, and NO<sub>3</sub><sup>-</sup> of the same concentration of 50 mg L<sup>-1</sup> was prepared to evaluate the phosphate uptake. The results are shown in Figure 6B, where L-

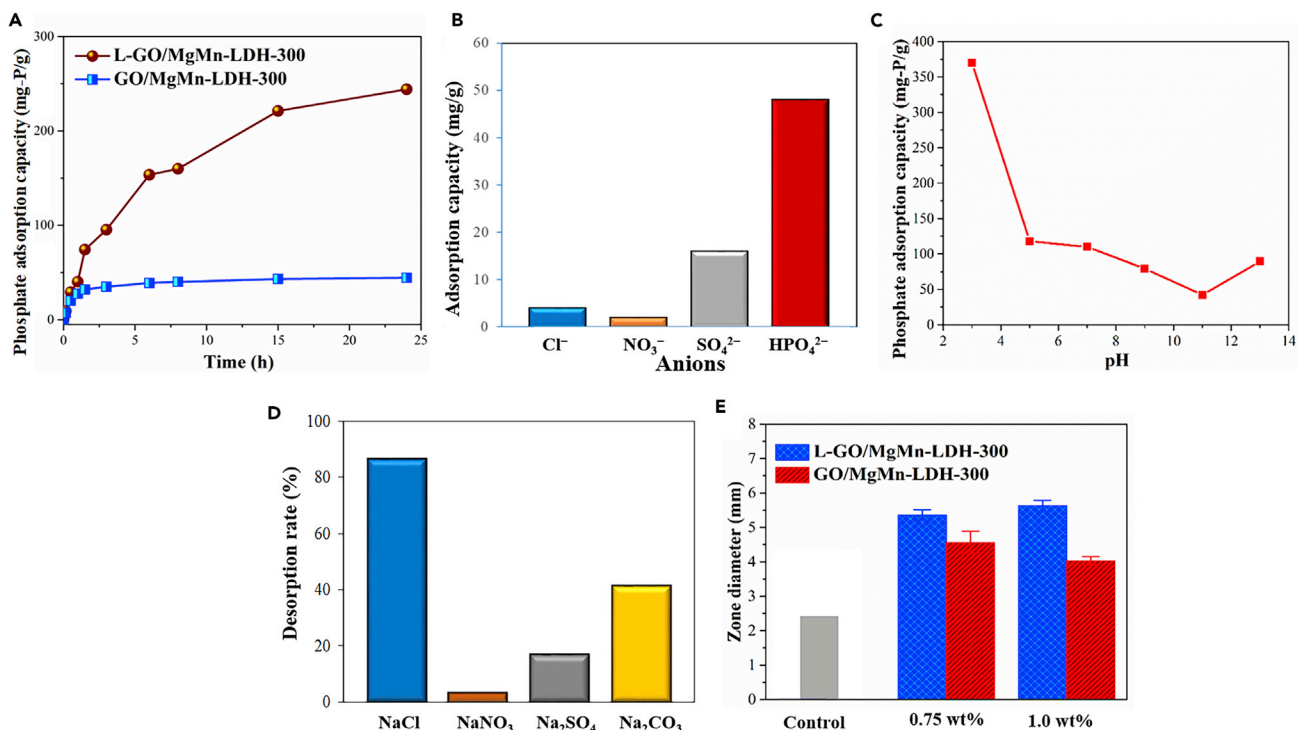


**Figure 6. The Practical Phosphate Sustainability by LDH Composites in Wastewater Treatment**

- (A) The phosphate adsorption capacities of GO/MgMn-LDH-300 and L-GO/MgMn-LDH-300 as a function of time. With the introduction of leaf-template, the LDH composite shows 5.5 times the phosphate adsorption capacity.
- (B) The selectivity of L-GO/MgMn-LDH-300 toward different ions.
- (C) The pH dependence of phosphate adsorption capacity of L-GO/MgMn-LDH-300.
- (D) The phosphate desorption test using 0.1 M NaOH solution in combination with the same concentration of different kinds of regenerating reagents. It indicates that 85.8% of desorption rate can be reached in a regeneration solution containing 0.1 M NaCl and NaOH.
- (E) The *E. coli* inhibition zones for L-GO/MgMn-LDH-300 and GO/MgMn-LDH-300 dispersions with concentrations of 0, 0.75, and 1.0 wt%. The enhanced antimicrobial ability of L-GO/MgMn-LDH-300 indicates that the proposed adsorbent is practical for phosphate sustainability in wastewater treatment application.

GO/MgMn-LDH-300 possessed high selectivity toward phosphate and resulted in higher adsorption capacity than other competing ions. The results agree with previous reports that higher-valence anions have stronger interaction with positively charged LDH sheets than monovalent anions (Goh et al., 2008). Moreover, HPO<sub>4</sub><sup>2-</sup> can form hydrogen bonds with aromatic hydrocarbons on biflavonoids and triterpenoids, which facilitate the selective adsorption of phosphate for L-GO/MgMn-LDH-300. The density functional theory (DFT) total energy calculations were performed to study selectivity of phosphate adsorption: HPO<sub>4</sub>, SO<sub>4</sub>, NO<sub>3</sub>, and Cl adsorbed on (on-phase) and away from (off-phase) the MgMn-LDH-biflavonoid system as shown in Figure S5. The adsorption energy of these molecules is thus the total energy difference between the on- and off-phase [E (off)-E (on)]. The calculated adsorption energies of HPO<sub>4</sub>, SO<sub>4</sub>, NO<sub>3</sub>, and Cl molecules are 1.43, 1.40, 0.73, and -2.63 eV, respectively. The HPO<sub>4</sub> molecule, superior to SO<sub>4</sub>, NO<sub>3</sub>, and Cl, shows the strongest tendency of adsorption on the MgMn-LDH-biflavonoid system.

In wastewater treatment, pH is an important parameter affecting the phosphate adsorption process. Herein, the adsorption of phosphate on L-GO/MgMn-LDH-300 was studied at different pH values ranging from 3.0 to 13.0. In Figure 6C, it can be observed that the phosphate adsorption capacity decreases with the increase in pH value from 3.0 to 11.0. As the pH value increases, the increasing competition between OH<sup>-</sup> and phosphate as well as the negatively charged surface results in lower phosphate adsorption on LDH composites (Li et al., 2016b). The lowest phosphate adsorption capacity is 42.2 mg-P/g around pH 11, which is higher than most of the results summarized in Table 2. It is noted that, as the solution pH rises to 13.0, the phosphate adsorption increases. Since phosphate is pH-related in solution, it exists differently as H<sub>2</sub>PO<sub>4</sub><sup>-</sup>, HPO<sub>4</sub><sup>2-</sup>, and PO<sub>4</sub><sup>3-</sup> with pK<sub>1</sub> = 2.12, pK<sub>2</sub> = 7.21, and pK<sub>3</sub> = 12.67, respectively (Yang et al., 2014). In the pH region above 12.67, PO<sub>4</sub><sup>3-</sup> is the dominant species, which has significant effects on the hydrogen bonding network (Tang et al., 2009). The presence of

Adsorbent	Pseudo-first-order			Pseudo-second-order		
	$q_e$ [mg-P/g]	$k_1$ [1/h]	$R^2$	$q_e$ [mg-P/g]	$k_2$ [g/mg-P h]	$R^2$
L-GO/MgMn-LDH-300	281.77	0.21233	0.9519	294.12	0.00062	0.9893
GO/MgMn-LDH-300	24.00	0.17157	0.9345	45.66	0.02694	0.9995

**Table 1. The Phosphate Adsorption Kinetic Models Parameters for L-GO/MgMn-LDH-300 and GO/MgMn-LDH-300 Composites**

orthophosphate can induce the formation of new interactions between P-O groups and hydrogen groups on biflavonoids and triterpenoids. The results indicate that L-GO/MgMn-LDH-300 has high phosphate adsorption in a wide range of pH, which can be applied to practical wastewater treatment.

To investigate the desorption behavior, the L-GO/MgMn-LDH-300 was treated with a  $\text{Na}_2\text{HPO}_4$  solution to obtain phosphate-loaded adsorbent, which possessed the phosphate uptake of  $150.91 \text{ mg-P g}^{-1}$ . The phosphate desorption test was performed using 0.1 M NaOH solution in combination with the same concentration of different kinds of regenerating reagents. After sonication for 6 h, the desorption results were shown in Figure 6D. The desorption rate reaches 85.8% in a regeneration solution containing 0.1 M NaCl and NaOH, which is much higher than other NaOH solutions mixed with  $\text{NaNO}_3$ ,  $\text{Na}_2\text{CO}_3$ , and  $\text{Na}_2\text{SO}_4$ , respectively. The results agree with the previous reports that LDHs have a high affinity for carbonate anions in the following order of valent state:  $\text{CO}_3^{2-} > \text{SO}_4^{2-} > \text{Cl}^- > \text{NO}_3^-$  (Seftel et al., 2018). The highest desorption rate using NaCl can be contributed from small ionic radius of  $\text{Cl}^-$  (Yan et al., 2018) and stable CH-Cl hydrogen bonds (de Medeiros et al., 2016), which facilitate intercalation into the LDHs to replace phosphate. In addition, the desorption rate can maintain more than 80% after three phosphate uptake-release cycles, as shown in Figure S6. The results show that the phosphate desorption efficiency and reusability of adsorbent can be enhanced in the presence of NaOH and NaCl.

Bacteria in wastewater not only make water recovery process difficult but also cause biofouling of adsorbent (Bhatti et al., 2018). Therefore, the antimicrobial ability is also an important key factor for wastewater treatment. The antimicrobial abilities of the GO/MgMn-LDH-300 and L-GO/MgMn-LDH-300 composites were determined by *Escherichia coli* through the disk-diffusion (Kirby-Bauer) method (shown in Figure S7). Figure 6E shows the inhibition zone diameters for LDH composite dispersions with different concentrations (the control group is 0.0 wt%). Both LDH composites possessed the inhibition zones, which might result from the composition of MgO. It is proposed that the MgO in aqueous suspension can produce superoxide ion of  $\text{O}_2^-$  and kill bacteria effectively (Huang et al., 2005). The results show that L-GO/MgMn-LDH-300 exhibit higher antimicrobial ability than GO/MgMn-LDH-300. More obvious difference of zone diameters can be observed when the concentration increases. The enhancement of antimicrobial ability for L-GO/MgMn-LDH-300 is due to the presence of *Garcinia subelliptica* leaves. *Garcinia subelliptica* leaves have been known to contain various kinds of chemical constituents, notably, biflavonoids and triterpenoids, which possess high antimicrobial activity through inhibition of *E. coli* DNA gyrase (Cushnie and Lamb, 2005; Inoue et al., 2017; Weng et al., 2003). The enhanced antimicrobial ability of L-GO/MgMn-LDH-300 indicates that the proposed work is practical for phosphate removal in wastewater treatment application.

### The Investigations of Selective Phosphate Adsorption

To further investigate the mechanism of selective phosphate adsorption by L-GO/MgMn-LDH-300, Raman mapping technique was used to characterize the P-L-GO/MgMn-LDH-300 surface in the region marked with blue dotted square in Figure 7A. Figure 7B illustrates the intensity distribution map of peak at  $945 \text{ cm}^{-1}$  (spectrum A in Figure 7D), which is assigned to P-O bond of  $\text{HPO}_4^{2-}$  stretching vibration in the phosphate absorbed by ion exchange (Frost et al., 2011). The broadening and unsymmetrical deformations of the P-O bond results from the interactions of hydrogen bonds with LDH composites (Syed et al., 2012). Figure 7C is the intensity distribution map of peak at  $429 \text{ cm}^{-1}$ , which is accompanied with an intensive band of  $578 \text{ cm}^{-1}$  (spectrum B in Figure 7D). The positions of these two bands, ranging between 400 and  $600 \text{ cm}^{-1}$ , are observed in typical LDH materials, which depends on the compositions of divalent and trivalent cations (Al-Jaberi et al., 2015; Cunha et al., 2012). These two bands are assigned to the  $\text{M}^{2+}\text{-O-M}^{3+}$  vibration modes and M-OH translation modes. The decreases of M-OH bands in spectrum A result from the ligand exchange of phosphate. Phosphate can form covalent bonds with metal cations while OH ions previously bonded to the metal cations are released (Seftel et al., 2018). It clearly shows that regions with the high-intensity peak of  $429 \text{ cm}^{-1}$  possess the low intensity of P-O bonds, indicating the non-specific active

Adsorbent	pH	Initial $\text{HPO}_4^{2-}$ Concentration (ppm)	Solution Volume (mL)	Adsorption Capacity (mg-P/g)	Reference
BR-LDH	7.0	100	50	18.6	Hu et al., 2017
RGO-Zr	5.0	10	200	27.7	Luo et al., 2016
MgAl-LDH	6.0–9.0	200	25	9.8	Yang et al., 2014
ZnAl-LDH	6.0–9.0	200	25	24.8	Yang et al., 2014
Mg/Al-LDH	9.0	9,600	200	57.3	Shimamura et al., 2012
Mg/Al-LDHs biochar	3.0	50	20	81.8	Li et al., 2016b
MgFe-Zr-LDH	7.0–8.0	10	100	30.0	Mandel et al., 2013
Lanthanum hydroxides	N.A.	200	40	107.5	Xie et al., 2014
Zn <sub>2</sub> Al-PMA-LDH	3.0	100	N.A.	76.0	Yu et al., 2015
MgMn-LDH-300	8.0	384	50	34.1	Satoko et al., 2004
GO/MgMn-LDH-300	6.7	50	200	44.5	This work
L-GO/MgMn-LDH-300	6.7	50	200	244.1	This work

**Table 2. Comparison of Phosphate Adsorption Capacity of This Work with Published Literature**

sites for selective phosphate adsorption. Figure 7D shows A and B Raman spectra of the selected regions in Figures 7B and 7C, respectively. The characteristic Raman bands at 665 cm<sup>-1</sup> in the high-frequency region is due to the Mn-O symmetric stretching vibrations  $A_g$  of  $\text{MnO}_2$  (Gao et al., 2009; Julien et al., 2003). The higher frequency and intensity of the Mn-O stretching vibration in A Raman spectrum can be ascribed to the change in the manganese oxidation state (Julien et al., 2003). In contrast, B Raman spectrum still possesses intensive typical LDH peaks ranging between 400 and 600 cm<sup>-1</sup>. These observations indicate that Mn oxidation progress to Mn<sup>4+</sup> during calcination can result in weakening the typical LDH structure and creating phosphate-specific active sites in L-GO/MgMn-LDH-300.

## DISCUSSION

This study proposes an eco-friendly adsorbent of L-GO/MgMn-LDH-300 composite, adopting *Garcinia subelliptica* leaves as an inexpensive and natural template, for the effective phosphate sustainability from wastewater. The presence of GO and *Garcinia subelliptica* leaves can not only form hierarchical porous structure but also provide more mesopores for efficient phosphate adsorption. By using *in situ* TEM, the mechanism of the phase transition of LDH composite was investigated. *Garcinia subelliptica* leaves contain biflavonoids and triterpenoids, which can intercalate into LDH layers and facilitate ion access to the LDH composite, leading to high phosphate adsorption capacity. In addition, the aromatic hydrocarbons and the lone pairs on biflavonoids and triterpenoids can form bondings to phosphate, resulting in high-phosphate-selective active sites. The antimicrobial ability of L-GO/MgMn-LDH is also enhanced. An efficient and recyclable selective phosphate adsorbent was proposed in this work, with a phosphate adsorption capacity and desorption rate of 244.08 mg-P g<sup>-1</sup> and 85.8%, respectively. The process offers a promising technique for the effective and economical phosphate recycling from aqueous solution, which is scalable, sustainable, and suitable in commercial wastewater treatment.

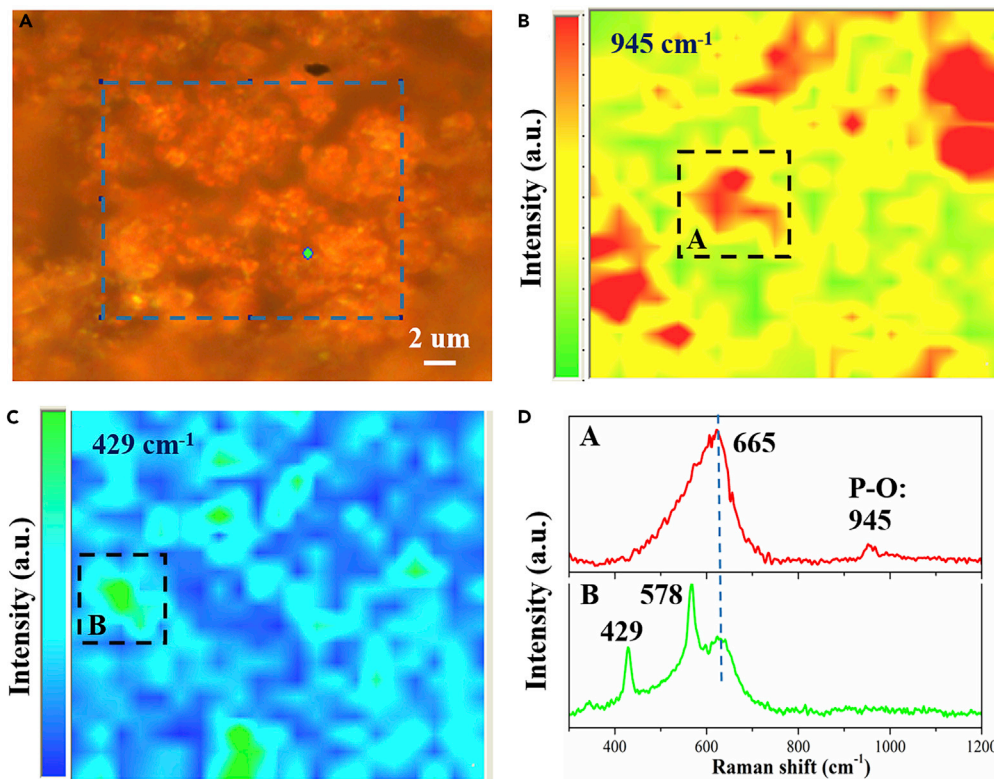


**Figure 7. Investigations of Selective Phosphate Adsorption**

(A) The optical microscope image of P-L-GO/MgMn-LDH-300. (B-D) The Raman mapping of selected regions marked in the blue dotted square in (A). (B)  $945\text{ cm}^{-1}$  and (C)  $429\text{ cm}^{-1}$ . (D) The selected A and B Raman spectra marked by black dotted squares in (B) and (C), respectively. It is noted that the region with higher intensive bands at  $665\text{ cm}^{-1}$  due to the Mn-O symmetric stretching vibrations has a higher intensive peak at  $429\text{ cm}^{-1}$  assigned to P-O bond. It indicates that the  $\text{Mn}^{4+}$  oxidation state can create more phosphate-specific active sites in L-GO/MgMn-LDH-300.

### Limitations of the Study

In this study, we investigated the performance of L-GO/MgMn-LDH-300 composite adopting *Garcinia subelliptica* leaves as bio-template for the effective phosphate sustainability from wastewater. The mechanism of the phase transition of LDH composite in the presence of GO and *Garcinia subelliptica* leaves was investigated using *in situ* TEM. Although the mechanism of selective phosphate adsorption was illustrated using Raman mapping technique, the resolution of Raman mapping is too rough to precisely distinguish the phosphate adsorption sites in nanoscale, as a result, the understanding of the phosphate adsorption of LDH composite can be enhanced with improved technique.

### METHODS

All methods can be found in the accompanying [Transparent Methods supplemental file](#).

### SUPPLEMENTAL INFORMATION

Supplemental Information can be found online at <https://doi.org/10.1016/j.isci.2020.101065>.

### ACKNOWLEDGMENTS

The authors thank the support from the National Tsing Hua University, Industrial Technology Research Institute, and Ministry of Science and Technology, Taiwan, under the contract of MOST 108-2917-I-007-009-. The antimicrobial ability investigation was conducted through the assistance of Li Ching, Kok, PhD student in Microbiology and Biotechnology Laboratory, Institute of Molecular Medicine, National Tsing

Hua University. H.-T.J. also thanks support from NCHC, CINC-NTU, AS-iMATE-109-13, and CQT-NTHU-MOE, Taiwan.

## AUTHOR CONTRIBUTIONS

Y.-T.L., designed the experiments. Y.-T.L., Y.-S.H. and Y.-C.L. conducted the experiments and analyzed the data. M.-C.C. helped measure the phosphate uptake and release. C.-H.C. and H.-T.J. conducted DFT calculations. Y.-T.L. and P.-C.H wrote the paper. All authors discussed the results and commented on the manuscript.

## DECLARATION OF INTERESTS

The authors declare no competing interests.

Received: October 10, 2019

Revised: March 15, 2020

Accepted: April 12, 2020

Published: May 22, 2020

## REFERENCES

- Al-Jaberi, M., Naille, S., Dossot, M., and Ruby, C. (2015). Interlayer interaction in Ca–Fe layered double hydroxides intercalated with nitrate and chloride species. *J. Mol. Struct.* 1102, 253–260.
- Arrabito, G., Bonasera, A., Prestopino, G., Orsini, A., Mattoccia, A., Martinelli, E., Pignataro, B., and Medaglia, G.P. (2019). Layered double hydroxides: a toolbox for chemistry and biology. *Crystals* 9, 361–403.
- Bai, L., Yuan, L., Ji, Y., and Yan, H. (2018). Effective removal of phosphate from aqueous by graphene oxide decorated with  $\alpha$ -Fe<sub>2</sub>O<sub>3</sub>: kinetic, isotherm, thermodynamic and mechanism study. *Arab. J. Sci. Eng.* 43, 3611–3620.
- Bhatti, H.T., Ahmad, N.M., Khan Niazi, M.B., Ur Rehman Alvi, M.A., Ahmad, N., Anwar, M.N., Cheema, W., Tariq, S., Batool, M., Aman, Z., et al. (2018). Graphene oxide-PES-based mixed matrix membranes for controllable antibacterial activity against *Salmonella typhi* and water treatment. *Int. J. Polym. Sci.* 2018, 12.
- Cheng, Y., Ying, Y., Japip, S., Jiang, S.-D., Chung, T.-S., Zhang, S., and Zhao, D. (2018). Advanced porous materials in mixed matrix membranes. *Adv. Mater.* 30, 1802401.
- Cunha, V.R.R., Petersen, P.A.D., Gonçalves, M.B., Petrilli, H.M., Taviot-Gueho, C., Leroux, F., Temperini, M.L.A., and Constantino, V.R.L. (2012). Structural, spectroscopic (NMR, IR, and Raman), and DFT investigation of the self-assembled nanostructure of pravastatin-LDH (layered double hydroxides) systems. *Chem. Mater.* 24, 1415–1425.
- Cushnie, T.P.T., and Lamb, A.J. (2005). Antimicrobial activity of flavonoids. *Int. J. Antimicrob. Agents* 26, 343–356.
- Davood Abadi Farahani, M.H., Hua, D., and Chung, T.-S. (2018). Cross-linked mixed matrix membranes (MMMs) consisting of amine-functionalized multi-walled carbon nanotubes and P84 polyimide for organic solvent nanofiltration (OSN) with enhanced flux. *J. Membr. Sci.* 548, 319–331.
- de Medeiros, V.C., de Andrade, R.B., Leitão, E.F.V., Ventura, E., Bauerfeldt, G.F., Barbatti, M., and do Monte, S.A. (2016). Photochemistry of CH<sub>3</sub>Cl: dissociation and CH···Cl hydrogen bond formation. *J. Am. Chem. Soc.* 138, 272–280.
- Dodds, W.K., Bouska, W.W., Eitzmann, J.L., Pilger, T.J., Pitts, K.L., Riley, A.J., Schloesser, J.T., and Thornbrugh, D.J. (2009). Eutrophication of U.S. freshwaters: analysis of potential economic damages. *Environ. Sci. Technol.* 43, 12–19.
- Frost, R.L., Palmer, S.J., and Xi, Y. (2011). A Raman spectroscopic study of the mono-hydrogen phosphate mineral dorfmanite Na<sub>2</sub>(PO<sub>3</sub>OH)·2H<sub>2</sub>O and in comparison with brushite. *Spectrochim. Acta A Mol. Biomol. Spectrosc.* 82, 132–136.
- Gao, T., Fjellvåg, H., and Norby, P. (2009). A comparison study on Raman scattering properties of  $\alpha$ - and  $\beta$ -MnO<sub>2</sub>. *Anal. Chim. Acta* 648, 235–239.
- Goh, K.-H., Lim, T.-T., and Dong, Z. (2008). Application of layered double hydroxides for removal of oxyanions: a review. *Water Res.* 42, 1343–1368.
- Gu, P., Zhang, S., Li, X., Wang, X., Wen, T., Jehan, R., Alsaedi, A., Hayat, T., and Wang, X. (2018). Recent advances in layered double hydroxide-based nanomaterials for the removal of radionuclides from aqueous solution. *Environ. Pollut.* 240, 493–505.
- Hu, P., Zhang, Y., Lv, F., Tong, W., Xin, H., Meng, Z., Wang, X., and Chu, P.K. (2017). Preparation of layered double hydroxides using boron mud and red mud industrial wastes and adsorption mechanism to phosphate. *Water Environ. J.* 31, 145–157.
- Huang, L., Li, D.Q., Evans, D.G., and Duan, X. (2005). Preparation of highly dispersed MgO and its bactericidal properties. *Eur. Phys. J. D* 34, 321–323.
- Inoue, T., Kainuma, M., Baba, K., Oshiro, N., Kimura, N., and Chan, E.W.C. (2017). *Garcinia subelliptica* Merr. (Fukugi): a multipurpose coastal tree with promising medicinal properties. *J. Intercult. Ethnopharmacol.* 6, 121–127.
- Ito, T., Yokota, R., Watarai, T., Mori, K., Oyama, M., Nagasawa, H., Matsuda, H., and Iinuma, M. (2013). Isolation of six isoprenylated biflavonoids from the leaves of *Garcinia subelliptica*. *Chem. Pharm. Bull.* 61, 551–558.
- Julien, C., Massot, M., Baddour-Hadjean, R., Franger, S., Bach, S., and Pereira-Ramos, J.P. (2003). Raman spectra of birnessite manganese dioxide. *Solid State Ionics* 159, 345–356.
- Kedar Kalyani Abhimanyu, J.R.B. (2012). Isolation and characterization of triterpenoids in cuticular wax of leaves of *Helianthus elasticus* Linn. (Loranthaceae) parasitic on *Memecylon umbellatum* Burm.f. (Melastomataceae). *Int. J. Drug Dev. Res.* 4, 243–251.
- Lai, Y.-T., Liu, W.-T., Chen, L.-J., Chang, M.-C., Lee, C.-Y., and Tai, N.-H. (2019a). Electro-assisted selective uptake/release of phosphate using a graphene oxide/MgMn-layered double hydroxide composite. *J. Mater. Chem. A* 7, 3962–3970.
- Lai, Y.-T., Liu, W.-T., Chung, L.-C., Liu, P.-I., Chang, M.-C., Horng, R.-Y., Chen, L.-J., Lee, C.-Y., and Tai, N.-H. (2019b). A facile microwave-assisted method to prepare highly electrosorptive reduced graphene oxide/activated carbon composite electrode for capacitive deionization. *Adv. Mater. Technol.* 4, 1900213.
- Li, B., Gu, Z., Kurniawan, N., Chen, W., and Xu, Z.P. (2017). Manganese-based layered double hydroxide nanoparticles as a T1-MRI contrast agent with ultrasensitive pH response and high relaxivity. *Adv. Mater.* 29, 1700373.
- Li, M., Liu, J., Xu, Y., and Qian, G. (2016a). Phosphate adsorption on metal oxides and metal hydroxides: a comparative review. *Environ. Rev.* 24, 319–332.
- Li, R., Wang, J.J., Zhou, B., Awasthi, M.K., Ali, A., Zhang, Z., Gaston, L.A., Lahori, A.H., and Maher, A. (2016b). Enhancing phosphate adsorption by Mg/Al layered double hydroxide functionalized biochar with different Mg/Al ratios. *Sci. Total Environ.* 559, 121–129.

Li, X., Xu, W., Tang, M., Zhou, L., Zhu, B., Zhu, S., and Zhu, J. (2016c). Graphene oxide-based efficient and scalable solar desalination under one sun with a confined 2D water path. *Proc. Natl. Acad. Sci. U.S.A.* 113, 13953.

Li, J., Wang, X., Zhao, G., Chen, C., Chai, Z., Alsaedi, A., Hayat, T., and Wang, X. (2018a). Metal-organic framework-based materials: superior adsorbents for the capture of toxic and radioactive metal ions. *Chem. Soc. Rev.* 47, 2322–2356.

Li, X., Li, J., Lu, J., Xu, N., Chen, C., Min, X., Zhu, B., Li, H., Zhou, L., Zhu, S., et al. (2018b). Enhancement of interfacial solar vapor generation by environmental energy. *Joule* 2, 1331–1338.

Li, X., Zhu, B., and Zhu, J. (2019). Graphene oxide based materials for desalination. *Carbon* 146, 320–328.

Lin, Y.-M., Song, C., and Rutledge, G.C. (2019). Direct Three-dimensional visualization of membrane fouling by confocal laser scanning microscopy. *ACS Appl. Mater. Interfaces* 11, 17001–17008.

Liu, C., Hsu, P.-C., Xie, J., Zhao, J., Wu, T., Wang, H., Liu, W., Zhang, J., Chu, S., and Cui, Y. (2017). A half-wave rectified alternating current electrochemical method for uranium extraction from seawater. *Nat. Energy* 2, 17007.

Liu, C., Wu, T., Hsu, P.-C., Xie, J., Zhao, J., Liu, K., Sun, J., Xu, J., Tang, J., Ye, Z., et al. (2019). Direct/alternating current electrochemical method for removing and recovering heavy metal from water using graphene oxide electrode. *ACS Nano* 13, 6431–6437.

Luo, X., Wang, X., Bao, S., Liu, X., Zhang, W., and Fang, T. (2016). Adsorption of phosphate in water using one-step synthesized zirconium-loaded reduced graphene oxide. *Sci. Rep.* 6, 39108.

Mandel, K., Drenkova-Tuhtan, A., Hutter, F., Gellermann, C., Steinmetz, H., and Sextl, G. (2013). Layered double hydroxide ion exchangers on superparamagnetic microparticles for recovery of phosphate from waste water. *J. Mater. Chem. A* 1, 1840–1848.

Mao, Jiajun, Tang, Yuxin, Wang, Yandong, Huang, Jianying, Dong, Xiuli, Chen, Zhong, and Lai, Yuekun (2019). Particulate Matter Capturing via Naturally Dried ZIF-8/Graphene Aerogels under Harsh Conditions. *iScience* 16, 133–144.

Ooi, K., Sonoda, A., Makita, Y., and Torimura, M. (2017). Comparative study on phosphate adsorption by inorganic and organic adsorbents from a diluted solution. *J. Environ. Chem. Eng.* 5, 3181–3189.

Peng, L., Dai, H., Wu, Y., Peng, Y., and Lu, X. (2018). A comprehensive review of phosphorus recovery from wastewater by crystallization processes. *Chemosphere* 197, 768–781.

Prestopino, G., Arrabito, G., Generosi, A., Mattoccia, A., Paci, B., Perez, G., Verona-Rinati, G., and Medaglia, P.G. (2019). Emerging switchable ultraviolet photoluminescence in dehydrated Zn/Al layered double hydroxide nanosheets. *Sci. Rep.* 9, 11498.

Ren, X., Yang, S., Tan, X., Chen, C., Sheng, G., and Wang, X. (2012). Mutual effects of copper and

phosphate on their interaction with  $\gamma$ -Al<sub>2</sub>O<sub>3</sub>: combined batch macroscopic experiments with DFT calculations. *J. Hazard. Mater.* 237–238, 199–208.

Sakulpaisan, S., Vongsetskul, T., Reamouppaturn, S., Luangkachao, J., Tantirungrotechai, J., and Tangboriboonrat, P. (2016). Titania-functionalized graphene oxide for an efficient adsorptive removal of phosphate ions. *J. Environ. Sci. Manag.* 167, 99–104.

Satoko, T., Ramesh, C., Kohji, S., Akinari, S., Kenta, O., and Tahei, T. (2004). The synthesis and phosphate adsorptive properties of Mg(II)–Mn(III) layered double hydroxides and their heat-treated materials. *Bull. Chem. Soc. Jpn.* 77, 2101–2107.

Setfel, E.M., Ciocarlan, R.G., Michielsen, B., Meynen, V., Mullens, S., and Cool, P. (2018). Insights into phosphate adsorption behavior on structurally modified ZnAl layered double hydroxides. *Appl. Clay Sci.* 165, 234–246.

Seviour, R.J., Mino, T., and Onuki, M. (2003). The microbiology of biological phosphorus removal in activated sludge systems. *FEMS Microbiol. Rev.* 27, 99–127.

Shao, M., Zhang, R., Li, Z., Wei, M., Evans, D.G., and Duan, X. (2015). Layered double hydroxides toward electrochemical energy storage and conversion: design, synthesis and applications. *Chem. Commun. (Camb.)* 51, 15880–15893.

Shchukarev, A.V., and Korolkov, D.V. (2004). XPS study of group IA carbonates. *Cent. Eur. J. Chem.* 2, 347–362.

Shimamura, A., Kanezaki, E., Jones, M.I., and Metson, J.B. (2012). Direct observation of grafting interlayer phosphate in Mg/Al layered double hydroxides. *J. Solid State Chem.* 186, 116–123.

Susi, T., Pichler, T., and Ayala, P. (2015). X-ray photoelectron spectroscopy of graphitic carbon nanomaterials doped with heteroatoms. *Beilstein J. Nanotechnol.* 6, 177–192.

Syed, K.A., Pang, S.-F., Zhang, Y., Zeng, G., and Zhang, Y.-H. (2012). Micro-Raman observation on the  $\text{HPO}_4^{2-}$  association structures in an individual dipotassium hydrogen phosphate ( $\text{K}_2\text{HPO}_4$ ) droplet. *J. Phys. Chem. A* 116, 1558–1564.

Tang, E., Di Tommaso, D., and de Leeuw, N.H. (2009). Hydrogen transfer and hydration properties of  $\text{HnPO}_4^{3-n}$  ( $n=0–3$ ) in water studied by first principles molecular dynamics simulations. *J. Chem. Phys.* 130, 234502.

Thong, Z., Cui, Y., Ong, Y.K., and Chung, T.-S. (2016). Molecular design of nanofiltration membranes for the recovery of phosphorus from sewage sludge. *ACS Sustain. Chem. Eng.* 4, 5570–5577.

Wan, C.F., and Chung, T.-S. (2018). Techno-economic evaluation of various RO+PRO and RO+FO integrated processes. *Appl. Energy* 212, 1038–1050.

Wang, Q., and O'Hare, D. (2012). Recent advances in the synthesis and application of layered double hydroxide (LDH) nanosheets. *Chem. Rev.* 112, 4124–4155.

Weng, J.-R., Lin, C.-N., Tsao, L.-T., and Wang, J.-P. (2003). Terpenoids with a new skeleton and

novel triterpenoids with anti-inflammatory effects from *Garcinia subelliptica*. *Chem. Eur. J.* 9, 5520–5527.

Wu, T., Liu, C., Kong, B., Sun, J., Gong, Y., Liu, K., Xie, J., Pei, A., and Cui, Y. (2019). Amidoxime-functionalized macroporous carbon self-refreshed electrode materials for rapid and high-capacity removal of heavy metal from water. *ACS Cent. Sci.* 5, 719–726.

Xie, J., Wang, Z., Lu, S., Wu, D., Zhang, Z., and Kong, H. (2014). Removal and recovery of phosphate from water by lanthanum hydroxide materials. *Chem. Eng. J.* 254, 163–170.

Xu, N., Li, Y., Zheng, L., Gao, Y., Yin, H., Zhao, J., Chen, Z., Chen, J., and Chen, M. (2014). Synthesis and application of magnesium amorphous calcium carbonate for removal of high concentration of phosphate. *Chem. Eng. J.* 251, 102–110.

Yan, H., Chen, Q., Liu, J., Feng, Y., and Shih, K. (2018). Phosphorus recovery through adsorption by layered double hydroxide nano-composites and transfer into a struvite-like fertilizer. *Water Res.* 145, 721–730.

Yan, Z., Zhu, B., Yu, J., and Xu, Z. (2016). Effect of calcination on adsorption performance of Mg-Al layered double hydroxide prepared by a water-in-oil microemulsion method. *RSC Adv.* 6, 50128–50137.

Yang, D., Fan, T., Zhang, D., Zhu, J., Wang, Y., Du, B., and Yan, Y. (2013). Biota templated hierarchical porous material: the positively charged leaf. *Chem. Eur. J.* 19, 4742–4747.

Yang, K., Yan, L.-G., Yang, Y.-M., Yu, S.-J., Shan, R.-R., Yu, H.-Q., Zhu, B.-C., and Du, B. (2014). Adsorptive removal of phosphate by Mg-Al and Zn-Al layered double hydroxides: kinetics, isotherms and mechanisms. *Sep. Purif. Technol.* 124, 36–42.

Yu, Q., Zheng, Y., Wang, Y., Shen, L., Wang, H., Zheng, Y., He, N., and Li, Q. (2015). Highly selective adsorption of phosphate by pyromellitic acid intercalated ZnAl-LDHs: assembling hydrogen bond acceptor sites. *Chem. Eng. J.* 260, 809–817.

Zhang, Y., Desmidt, E., Van Looveren, A., Pinoy, L., Meesschaert, B., and Van der Bruggen, B. (2013). Phosphate separation and recovery from wastewater by novel electrodialysis. *Environ. Sci. Technol.* 47, 5888–5895.

Zhang, Yaxin, Ravi, Sai Kishore, Vaghasiya, Jayraj Vinubhai, and Tan, Swee Ching (2018). A Barbeque-Analog Route to Carbonize Moldy Bread for Efficient Steam Generation. *iScience* 3, 31–39.

Zhao, G., Huang, X., Tang, Z., Huang, Q., Niu, F., and Wang, X. (2018). Polymer-based nanocomposites for heavy metal ions removal from aqueous solution: a review. *Polym. Chem.* 9, 3562–3582.

Zhou, J., Yang, S., Yu, J., and Shu, Z. (2011). Novel hollow microspheres of hierarchical zinc-aluminum layered double hydroxides and their enhanced adsorption capacity for phosphate in water. *J. Hazard. Mater.* 192, 1114–1121.

## **Supplemental Information**

**Green Treatment of Phosphate from Wastewater**

**Using a Porous Bio-Templated Graphene**

**Oxide/MgMn-Layered Double Hydroxide Composite**

**Yi-Ting Lai, Yu-Sheng Huang, Chin-Hsuan Chen, Yan-Cheng Lin, Horng-Tay Jeng, Min-Chao Chang, Lih-Juann Chen, Chi-Young Lee, Po-Chun Hsu, and Nyan-Hwa Tai**

## Supplemental Information

### Transparent Methods

**Materials:** GO was synthesized from nature graphite powder (325 mesh, Alfa Aesar) according to our previous study.<sup>[1]</sup> The GO was uniformly dispersed in 200 mL of DI water ( $1 \text{ mg mL}^{-1}$ ) to obtain GO suspension. Fresh *Garcinia subelliptica* leaves were immersed in 95% ethanol solution and sonicated for 2 h and then dried at 70°C to remove excess liquid. Subsequently, the leaves were ground by ball milling process to obtain *Garcinia subelliptica* leaf powder. The leaf powder was then added into GO suspension ( $2 \text{ mg mL}^{-1}$ ) to obtain leaf-template GO (L-GO) suspension. The L-GO suspension was then added to a 200 mL solution of 0.2 M NaOH and 0.1 M Na<sub>2</sub>CO<sub>3</sub>. Subsequently, a 200 mL solution of 0.03 M MgCl<sub>2</sub> and 0.01 M MnCl<sub>2</sub> was added dropwise to the above solution. After stirring for 4 h, the mixture was then precipitated and washed repeatedly with DI water until neutral. The precipitation was subjected to freeze-dried process subsequently to obtain L-GO/MgMn-LDH (Mg/Mn = 3) powder. The calcined products were prepared by heating the L-GO/MgMn-LDH at 300°C in air for 4 h to produce L-GO/MgMn-LDH-300. For comparison, GO/MgMn-LDH and its calcined form were synthesized according to the method proposed by our previous work.<sup>[2]</sup>

**Characterizations:** The film morphology and microstructure of the samples were characterized using a field emission scanning electron microscope (FESEM, JEOL JSM-6500F) and a transmission electron microscope (TEM; JEM 3000F), respectively. TEM (JEOL JEM 2000V, base pressure  $\sim 5 \times 10^{-8} \text{ Pa}$ ) was used to heat the samples *in situ* to observe the hierarchical pores formation in nanoscale. The phase structure was verified using powder X-ray diffraction (PXRD, D2 PHASER, Bruker). A Raman spectroscope (Horiba Jobin Yvon LABRAM HR 800 UV) equipped with a 532 nm Ar<sup>+</sup> laser was used to characterize the chemical bonds, groups of bonds. The chemical states of the materials were measured using X-ray photoelectron spectroscope (XPS, ESCA Ulvac-PHI PHI 1600). A Fourier transform infrared spectrometer (FTIR, Thermo Scientific Nicolet iS 5, Germany) was also used for function group identification. The specific surface areas of the samples were measured using a surface area analyzer (Micromeritics Tristar II 3020) based on the Brunauer–Emmett–Teller (BET) method.

**Thermal process using *in situ* TEM:** *In situ* TEM was used to heat the samples *in situ* to observe the hierarchical pores formation in nanoscale. The thermal treatment of the sample was carried out with the heating element built in the double tilt heating holder (JEOL EM-21240) and gradually heated to 200°C in 30 min. After maintaining the temperature for 30 min, the sample was slowly heated to 300°C and subsequently maintained the temperature for 100 min and calibrated with an infrared pyrometer. The variation of nanostructure during thermal process using *in situ* TEM was recorded as a video and provided as supplemental information.

**Measurements of phosphate uptake and release:** A 200 mL phosphate solution with  $50 \text{ mg L}^{-1}$  was prepared by adding appropriate Na<sub>2</sub>HPO<sub>4</sub> to evaluate selectivity of phosphate uptake by LDH composites. Certain amount of adsorbent was adopted and stirred in phosphate solution with appropriate concentration, which the phosphate concentrations were calculated at different time. For the desorption process, the phosphate-adsorbed LDH composites were dispersed in a regeneration solution containing 0.1 M NaCl and NaOH and sonicated for 6 h to investigate the regeneration of LDH composites. Phosphate concentrations of solutions were measured using an ion chromatograph (IC) with 70 mM Na<sub>2</sub>CO<sub>3</sub> and 20 mM NaHCO<sub>3</sub> as the eluent (Dionex ICS-1000, Dionex Aquion, USA) and an IonPac AS14 analytical column (4 mm × 250 mm). The flow rate of the eluent was 1 mL/min with a sample injection volume of 25 μL. Standard solutions containing an equal ratio of phosphate and sulfate at concentrations of 0.625, 1.25, 2.5, 5.0 and 10.0 mg L<sup>-1</sup> were prepared for each measurement. Phosphate uptake and release were calculated based upon the difference in phosphate concentration relative to its initial concentration. Adsorption and desorption capacity (mg-

P g<sup>-1</sup>) was calculated based on the mass ratio of the uptake and release phosphate and the adsorbents, respectively.

*The antimicrobial ability study:* The antimicrobial abilities of the GO/MgMn-LDH-300 and L-GO/MgMn-LDH-300 composites were tested by the disk-diffusion (Kirby–Bauer) method. *Escherichia coli* (*E. coli*) was incubated in the Luria Broth (LB) media and shaken under 200 rpm at 310 K for 24 h, followed by dilution with the LB medium to the concentrations of 10<sup>6</sup> cfu mL<sup>-1</sup>. The GO/MgMn-LDH-300 and L-GO/MgMn-LDH-300 dispersions with 0.75 and 1.0 wt% were added to the filter papers and put in the LB agar plates, respectively. The plates were incubated in incubator at 310 K for 24 h, and the inhibition zones were determined.

*Density functional theory (DFT) total energy calculations:* First-principles calculations were performed using the projected augmented wave method (PAW)<sup>[3]</sup> as implemented in the Vienna Ab initio Simulation Package (VASP)<sup>[4]</sup> based on density functional theory (DFT) with the Perdew–Burke–Ernzerhof (PBE) type of generalized gradient approximation (GGA). The cutoff energy of 300 eV are used in the self-consistent field calculations over the 3x3x1 k-point mesh. The MgMn-LDH and biflavonoid lattice structure are optimized with the total energies converged within 10<sup>5</sup> eV.

**Table S1. Textural properties of LDH composite materials, related to 2F.**

Materials	BET surface area [m <sup>2</sup> g <sup>-1</sup> ]	Total pore volume [cm <sup>3</sup> g <sup>-1</sup> ]	Mesopore volume [cm <sup>3</sup> g <sup>-1</sup> ]	Mesopore ration [%]	Average pore size [nm]
L-GO/MgMn-LDH	17.45	0.07	0.04	57.14	12.24
L-GO/MgMn-LDH-300	91.39	0.24	0.21	87.50	8.95
GO/MgMn-LDH-300	71.10	0.21	0.17	80.95	11.35

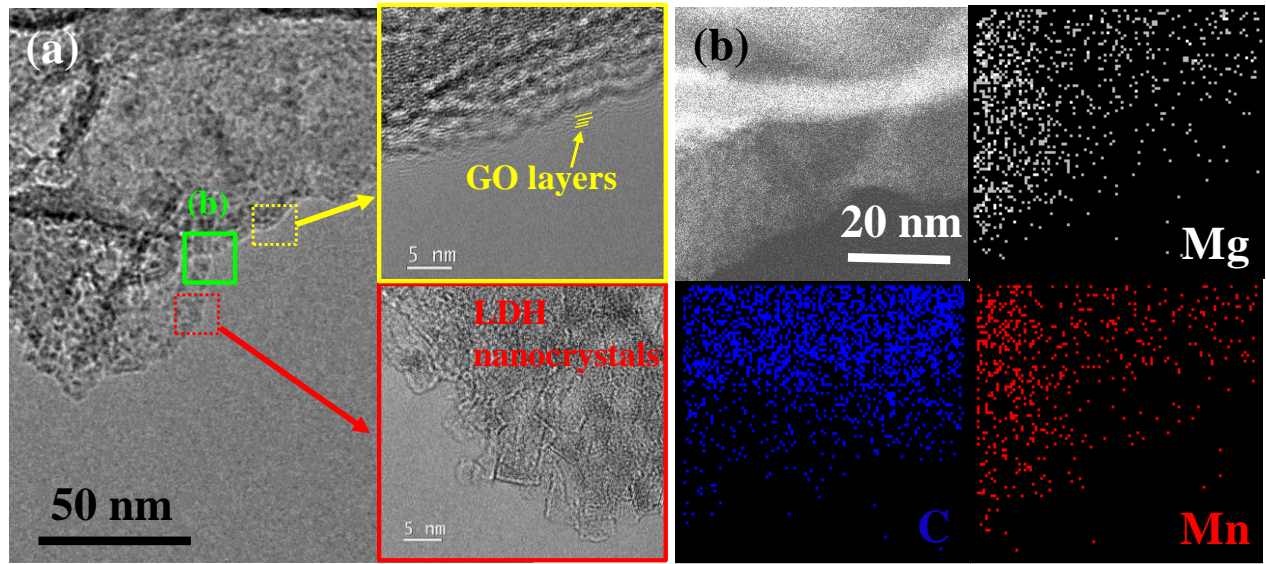


**Figure S1. The morphology and elements distributions of LDH composite, related to Figure 2D.**

(A) TEM image and HRTEM images (in the insets) show that L-GO/MgMn-LDH composite contained GO layers and MgMn-LDH nanocrystals. The HRTEM images in the upper right yellow and lower right red inset indicate the few layers of GO and plate-like nanocrystals of MgMn-LDH, respectively.

(B) The selected green area in Figure S1A of energy dispersive X-ray spectroscope (EDS) mapping analyses of C, Mg and Mn element distributions. It reveals that the plate-like nanocrystals with high concentrations of Mg and Mn elements can be referred to as MgMn-LDH. The homogeneous distribution of C element demonstrates that GO was uniformly coated on the L-GO/MgMn-LDH-300 composites surface.

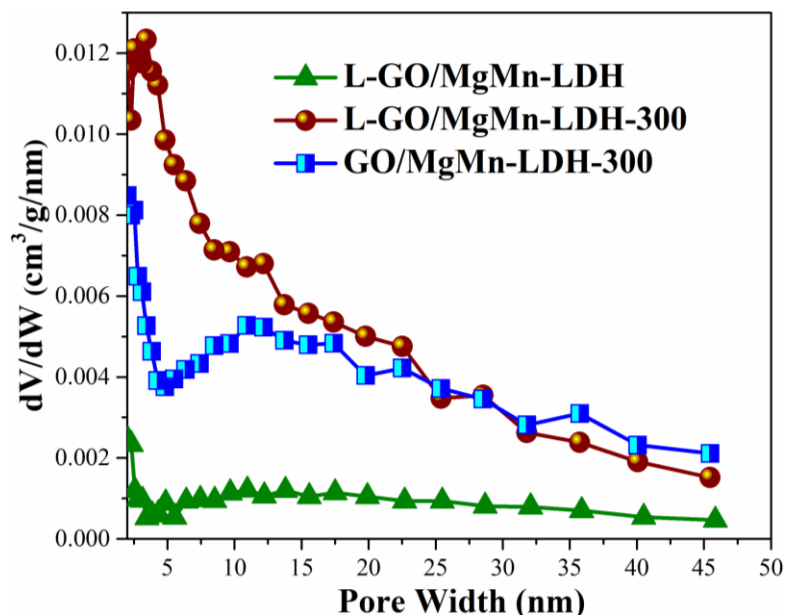


**Figure S2. Characteristics of the volume of mesopores of LDH composites, related to Figure 2F.** Mesopore size distribution curves of LDH composites. The L-GO/MgMn-LDH-300 possesses a high volume of mesopores.

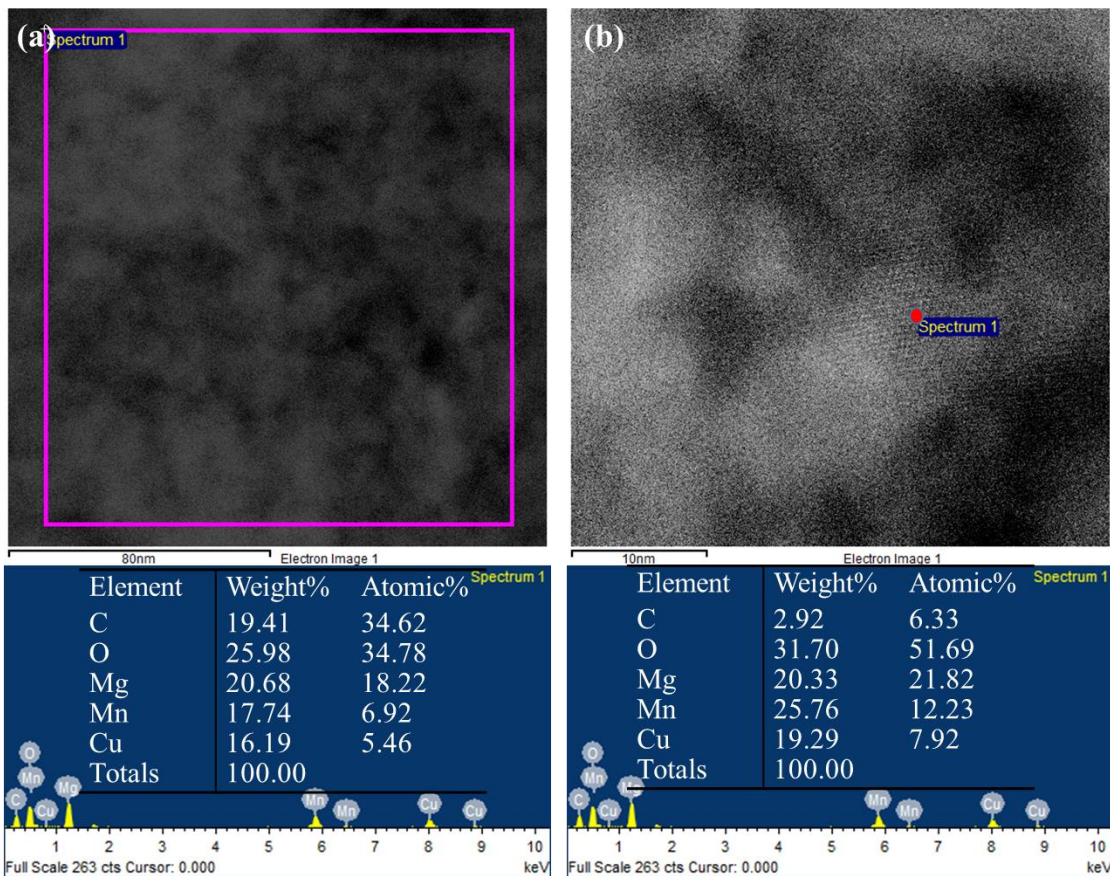


**Figure S3. Characteristics of elements distributions of LDH composite, related to Figure 4C.**  
 (A) The EDS spectra for elemental analysis of the large area and (B) the crystallization part of L-GO/MgMn-LDH-300 composite. It clearly shows that the Mg:Mn ratio of crystallization part decreased to near 2:1, which resulted from the formation of  $\text{Mg}_2\text{MnO}_4$ .

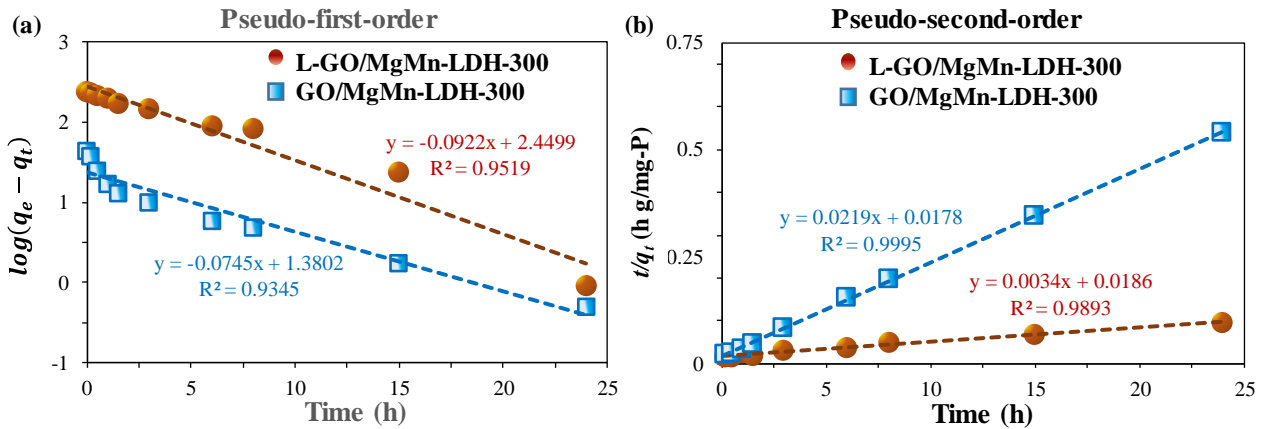


**Figure S4.** The phosphate adsorption capacity and kinetics of LDH composites, related to Figure 6A and Table 1.

(A) The pseudo-first-order kinetic and (B) pseudo-second-order kinetic curves fitting for phosphate adsorption by L-GO/MgMn-LDH-300 and GO/MgMn-LDH-300 composites. The pseudo-first-order and pseudo-second-order equations were used to study the adsorption kinetics of phosphate and were listed in equations (1) and (2), respectively:<sup>[5]</sup>

$$\log(q_e - q_t) = \log q_e - \frac{k_1}{2.303} t \quad (1)$$

$$\frac{t}{q_t} = \frac{1}{k_2 q_e^2} + \frac{t}{q_e} \quad (2)$$

where  $q_e$  (mg-P/g) is the phosphate adsorption capacity at equilibrium,  $q_t$  (mg-P/g) is the phosphate adsorption capacity at time  $t$  (h).  $k_1$  (1/h) and  $k_2$  (g/(mg-P h)) are the rate constant of pseudo-first-order and pseudo-second-order models, respectively. Parameters of both kinetic model were fitted to the experimental data of phosphate adsorption capacities, and the results are summarized in Table 1. The results show that higher correlation coefficients ( $R^2$ ) of pseudo-second-order model is appropriate to describe the phosphate adsorption kinetics for both adsorbents. It suggests that the phosphate adsorption process of LDH compositeds is dominated by chemisorption.

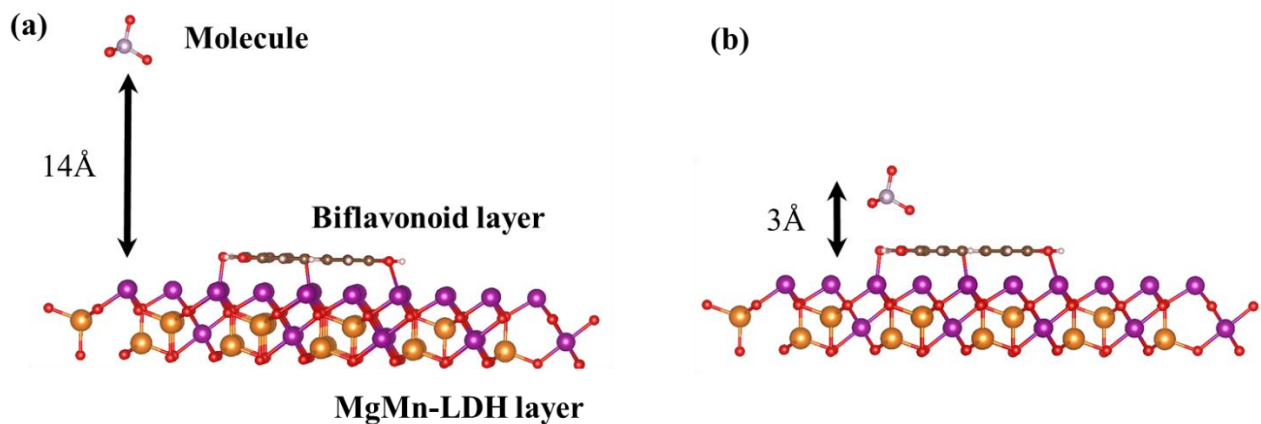


**Figure S5. Density functional theory (DFT) total energy calculations, related to Figure 6B.**

(A) The molecule away (off-phase) from the MgMn-LDH-biflavonoid system and (B) adsorbed (on-phase) on the MgMn-LDH-biflavonoid system. The adsorption energy difference of 4 molecules: HPO<sub>4</sub>, SO<sub>4</sub>, NO<sub>3</sub>, and Cl are calculated as 1.42, 1.40, 0.73, and -2.63 eV, respectively.

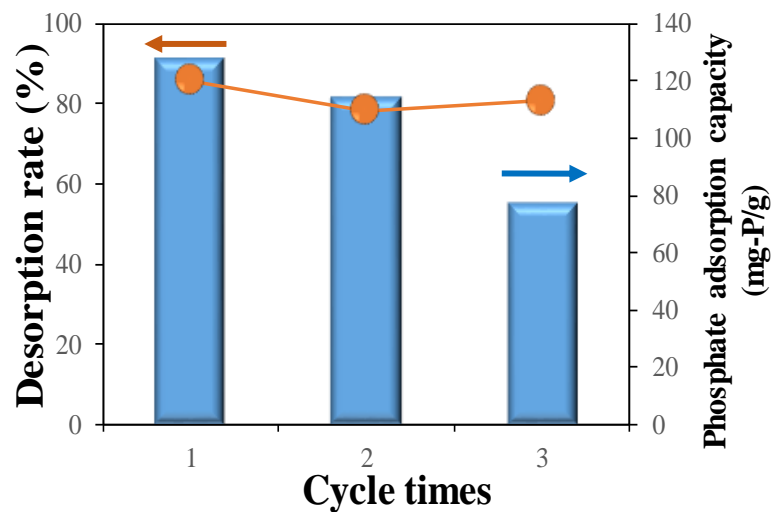


**Figure S6. Phosphate recovery cycle tests by L-GO/MgMn-LDH-300 composite, related to Figure 6D.** Recovery percentage of phosphate adsorbed by L-GO/MgMn-LDH-300 with three cycle times.

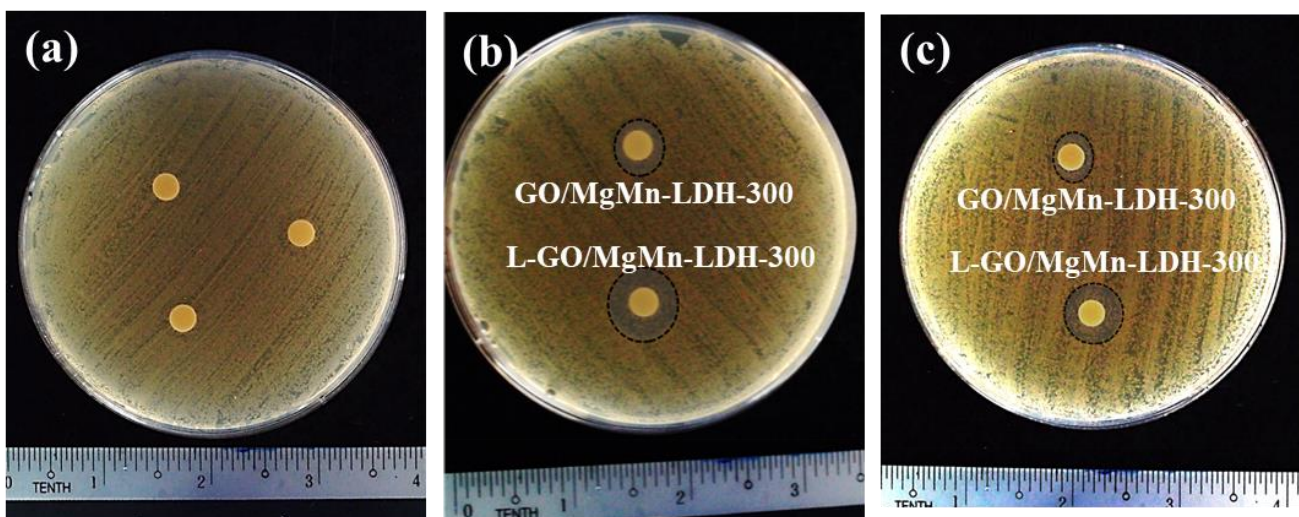


**Figure S7. The antimicrobial ability tests by *Escherichia coli* (*E. coli*) through the disk-diffusion (Kirby-Bauer) method, related to Figure 6E.** The *E. coli* inhibition zones for L-GO/MgMn-LDH-300 and GO/MgMn-LDH-300 dispersions with concentrations of (A) 0.0, (B) 0.75 and (C) 1.0 wt%.

#### Supplemental References

- [1] D. D. Nguyen, Y.-T. Lai, N.-H. Tai, Diamond and Related Materials 2014, 47, 1.
- [2] Y.-T. Lai, W.-T. Liu, L.-J. Chen, M.-C. Chang, C.-Y. Lee, N.-H. Tai, Journal of Materials Chemistry A 2019, 7, 3962.
- [3] P. E. Blöchl, Physical Review B 1994, 50, 17953; G. Kresse, D. Joubert, Physical Review B 1999, 59, 1758.
- [4] G. Kresse, J. Hafner, Physical Review B 1993, 47, 558; G. Kresse, J. Hafner, Physical Review B 1994, 49, 14251; G. Kresse, J. Furthmüller, Physical Review B 1996, 54, 11169; G. Kresse, J. Furthmüller, Computational Materials Science 1996, 6, 15.
- [5] K. Yang, L.-g. Yan, Y.-m. Yang, S.-j. Yu, R.-r. Shan, H.-q. Yu, B.-c. Zhu, B. Du, Separation and Purification Technology 2014, 124, 36.